Joule

CellPress

Report

Solar Water Splitting with Perovskite/Silicon Tandem Cell and TiC-Supported Pt Nanocluster Electrocatalyst

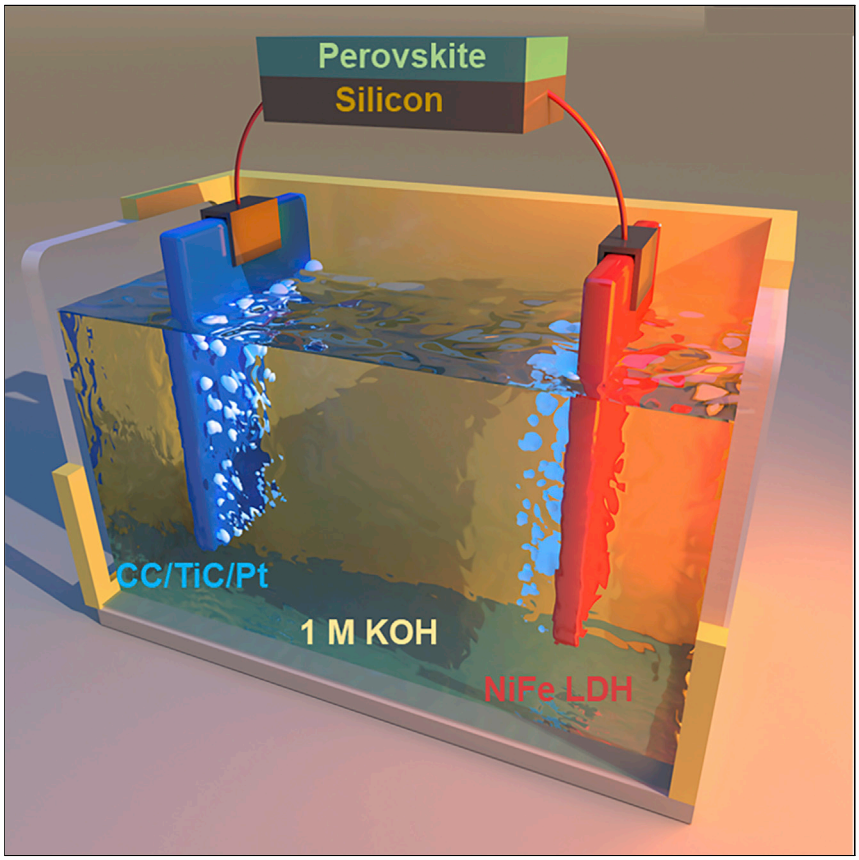

A highly efficient solar water splitting system using TiC supported Pt nanocluster catalyst for hydrogen evolution and nickel-iron layered double hydroxide catalyst for oxygen evolution and driven by a monolithic perovskite/silicon tandem cell.

Jing Gao, Florent Sahli, Chenjuan Liu, ..., Christophe Ballif, Michael Grätzel, Jingshan Luo

michael.graetzel@epfl.ch (M.G.)
jingshan.luo@nankai.edu.cn (J.L.)

HIGHLIGHTS

Development of TiC/Pt catalyst rivaling the performance of commercial Pt/C

Achievement of a highly efficient water electrolyzer with TiC/Pt and NiFe LDH

Achievement of 18.7% solar-driven water splitting

Gao et al., Joule 3, 2930–2941
December 18, 2019
https://doi.org/10.1016/j.joule.2019.10.002

Joule

CellPress

Report

Solar Water Splitting with Perovskite/Silicon Tandem Cell and TiC-Supported Pt Nanocluster Electrocatalyst

Jing Gao,[1,3] Florent Sahli,[4] Chenjuan Liu,[5] Dan Ren,[1] Xueyi Guo,[3] Jérémie Werner,[4] Quentin Jeangros,[4] Shaik Mohammed Zakeeruddin,[1] Christophe Ballif,[4] Michael Grätzel,[1,*] and Jingshan Luo[2,1,6,*]

SUMMARY

Developing efficient, stable, and cost-effective photosystems to split water into hydrogen and oxygen using sunlight is of paramount importance for future production of fuels and chemicals from renewable sources. However, the high cost of current systems limits their widespread application. Here, we developed a highly efficient TiC-supported Pt nanocluster catalyst for hydrogen evolution reaction that rivals the commercial Pt/C catalyst with ~5 times less Pt loading. Combining with the NiFe-layered double hydroxide for oxygen evolution reaction and driven for the first time by a monolithic perovskite/silicon tandem solar cell, we achieved a solar water splitting system with 18.7% solar-to-hydrogen conversion efficiency, setting a record for water splitting systems with earth-abundant and inexpensive photo-absorbers.

INTRODUCTION

The world's increasing energy consumption leads to the fast depletion of fossil fuels along with devastating environmental effects that warrant their rapid replacement by renewable sources such as solar, hydroelectricity, and wind.[1–4] Due to their intermittent nature, an energy carrier is required for the ease of usage, storage, and transportation. Hydrogen is an attractive candidate to assume this function and can be generated via water splitting driven by solar energy or other forms of renewable electricity.[5–8]

Among the approaches explored for solar-triggered hydrogen generation, water electrolysis driven by photovoltaics (PVs) has exhibited the highest efficiencies so far,[9] as shown in the summary of recent PV-driven electrolysis systems (Table S1). The highest solar-to-hydrogen (STH) conversion efficiency demonstrated to date was 30%, achieved by coupling InGaP/GaAs/GaInNAsSb triple-junction solar cell with two series-connected polymer electrolyte membrane (PEM) electrolyzers.[10] However, it was obtained under concentrated illumination condition, and so were many other systems.[11,12] Recently, Cheng et al. reported a STH conversion efficiency of 19.3% under standard AM 1.5 G solar radiation using a III-V semiconductor-based tandem cell combined with Rh and RuO_x catalysts for the hydrogen evolution reaction (HER) and oxygen evolution reaction (OER), respectively.[13] However, the scarcity and high cost of the III-V semiconductors and noble-metal-based catalysts preclude the widespread use of such systems.

Perovskite solar cells (PSCs) have recently emerged as an attractive contender for low-cost photovoltaics, reaching a certified power conversion efficiency of

Context & Scale

Solar energy is of paramount importance for realizing a clean and renewable energy future. Due to its intermittency, an energy storage system is generally demanded. Hydrogen production via solar water splitting is a promising approach to store solar energy and realize a carbon-neutral economy. Here, we present an exciting process toward a highly efficient solar water splitting system at an affordable cost using TiC-supported Pt nanocluster electrocatalysts and monolithic perovskite/silicon tandem cells, which will help to bring the hydrogen economy closer to reality.

25.2%.[14] However, the voltage of highly efficient PSCs at their maximum power point remains below the minimum of 1.23 V required for driving water electrolysis. To meet this voltage need, we previously connected two PSCs in series, attaining an STH efficiency of 12.3%,[15] whereas an efficiency of 14.2% was reported when using three silicon solar cells connected in series.[16]

Here, we introduce a 2-terminal perovskite/monocrystalline silicon (perovskite/Si) tandem solar cell with a V_{oc} of 1.76 V as a low-cost alternative to III-V multi-junction solar cells to drive water splitting.[17] Water photo-electrolysis was carried out in an alkaline electrolyte using highly dispersed platinum (Pt) nanoclusters and NiFe-layered double hydroxide (LDH) as catalysts for the HER and OER, respectively. Even though various kinds of earth-abundant electrocatalysts have been developed for the HER, such as MoS_2,[18] Mo_2C,[19] and Ni_2P[20] in acidic solution as well as Ni/NiO,[21] NiMo,[22] and CoS_2[23] in alkaline condition, their performance remains inferior to Pt, which remains to date the most active hydrogen evolution catalyst.[24] To reduce substantially the quantity of Pt employed in the electrolyzer and hence its cost, we downsized the catalyst particles to the single-atom or nanocluster scale. This increases the dispersion and activity for the same catalyst loading since a larger fraction of under-coordinated or unsaturated Pt atoms is exposed compared to bulk atoms.[25–28] For example, isolated single atoms of Pt immobilized on FeO_x have shown excellent stability and high activity for CO oxidation and nitroarene hydrogenation.[29]

We prepared the Pt nanocluster catalyst on different supports and tested the effect of the substrate material on their HER activity. It is found out that Pt nanocluster deposited on TiC nanowires (NWs), which are in turn supported on a carbon cloth, exhibited the best catalytic activity and stability toward HER in both alkaline and acidic electrolytes, matching the performance of commercial Pt/C catalysts at ~5 times less Pt loading. Combining a TiC/Pt and NiFe LDH as HER and OER catalyst, respectively, an alkaline electrolyzer and a perovskite/Si tandem solar cell to drive water splitting, we achieve an STH efficiency of 18.7%.

RESULTS

Pt nanoclusters were deposited by atomic layer deposition (ALD) onto three different substrates: commercial carbon cloth (CC), carbon cloth coated by a TiO_2 layer (CC/TiO_2) and TiC nanowire arrays grown on carbon cloth (CC/TiC). We coated the TiO_2 films with a thickness of 30 nm by ALD, followed by thermal annealing at 900°C in Ar atmosphere. CC/TiC was prepared by annealing graphite and TiO_2 on the carbon cloth substrate. The morphology of the substrates was characterized by scanning electron microscopy (SEM; Figure S1). We observed a continuous polycrystalline TiO_2 film with apparent grain boundaries covering the surface of the carbon cloth, while the CC/TiC presents an abundance of nanowires with a diameter of 300–500 nm (Figures S1C and S1D).

Atomic layer deposition of 3-nm-thick Pt results in the formation of discrete nanoclusters with a size of ~2–5 nm, uniformly dispersed on the surface of the three substrates without agglomeration (Figures 1A–1C). The deposition of thicker (8 nm) Pt layers leads to the formation of larger nanoparticles (Figure S2). Unless otherwise stated, all the catalysts referred to below were produced from the 3-nm-thick Pt deposition by ALD. The calculated mass loadings of 3-nm-thick Pt on CC, CC/TiO_2, and CC/TiC are 0.199, 0.175, and 0.202 mg cm^{-2}, respectively (Table S2; see calculation in Experimental Procedures).

[1]Laboratory of Photonics and Interfaces, École Polytechnique Fédérale de Lausanne, Lausanne 1015, Switzerland

[2]Institute of Photoelectronic Thin Film Devices and Technology, Key Laboratory of Photoelectronic Thin Film Devices and Technology of Tianjin, Nankai University, Tianjin 300350, China

[3]School of Metallurgy and Environment, Central South University, Changsha, Hunan 410083, China

[4]Photovoltaics and Thin Film Electronics Laboratory, École Polytechnique Fédérale de Lausanne, 2002 Neuchâtel, Switzerland

[5]Department of Chemistry, Ångström Laboratory, Uppsala University, Box 538, SE-75121 Uppsala, Sweden

[6]Lead Contact

*Correspondence: michael.graetzel@epfl.ch (M.G.), jingshan.luo@nankai.edu.cn (J.L.)

https://doi.org/10.1016/j.joule.2019.10.002

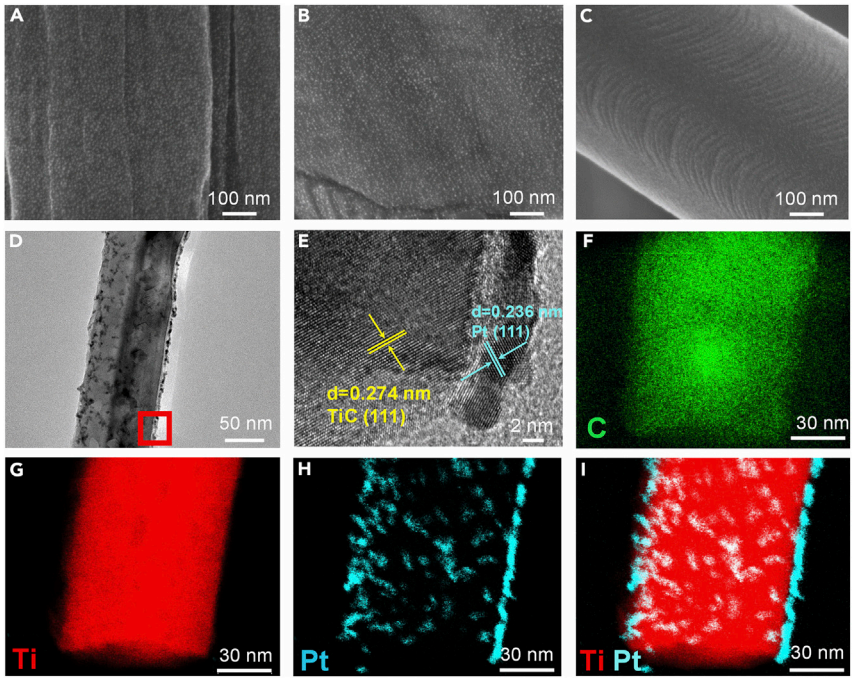

Figure 1. Morphological Characterization of the Electrocatalysts

SEM images of (A) CC/Pt, (B) CC/TiO_2/Pt, (C) CC/TiC/Pt, (D) TEM, and (E) high-resolution TEM images of CC/TiC/Pt; STEM EDX chemical maps for (F) C, (G) Ti, (H) Pt, and (I) Ti and Pt of a representative CC/TiC/Pt nanowire.

We carried out transmission electron microscopy (TEM) and energy-dispersive X-ray spectroscopy (EDX) elemental mapping coupled with scanning transmission electron microscopy (STEM) to characterize the CC/TiC/Pt catalyst (Figures 1D–1I). Discrete Pt nanoclusters were anchored on the surface of TiC nanowires. The lattices of 0.236 nm and 0.274 nm correspond to the (111) lattice planes of Pt and TiC, respectively. The elemental maps of CC/TiC/Pt further confirmed the uniform distribution of Pt nanoclusters on the surface of TiC nanowires.

Hydrogen Evolution on Pt Nanocluster Catalysts

The electrocatalytic hydrogen evolution activity of the Pt nanocluster catalysts coated on different substrates was characterized by linear sweep voltammetry (LSV) at a scan rate of 1 mV s^{-1} in both aqueous 0.5 M H_2SO_4 (Figure 2A) and 1 M KOH solutions (Figure 2B). In acidic electrolyte, CC/TiC/Pt exhibited the lowest overpotential (35 mV) to deliver a current density of −10 mA cm^{-2}, followed by CC/TiO_2/Pt (50 mV) and CC/Pt (54 mV). The Tafel slopes of the CC/TiO_2/Pt and CC/TiC/Pt catalysts were ~30 mV dec^{-1} (Figure S3A) in 0.5 M H_2SO_4, indicating that the HER follows a Tafel-Volmer mechanism with Tafel reaction as the rate-determining step.[30,31]

In basic electrolyte, the CC/TiC/Pt catalyst showed a higher activity than CC/Pt and CC/TiO_2/Pt (Figure 2B), delivering a current density of −10 mA cm^{-2} at an overpotential of only 37 mV, which is 19–27 mV below the overpotential needed for the other two supports, respectively. All the catalysts showed a Tafel slope of ~60 mV dec^{-1} (Figure S3B), indicating that the hydrogen generation from these catalysts goes through a Heyrovsky-Volmer mechanism with the Heyrovsky step as the rate-determining step. Note that increasing the thickness of the Pt layer to >3 nm has

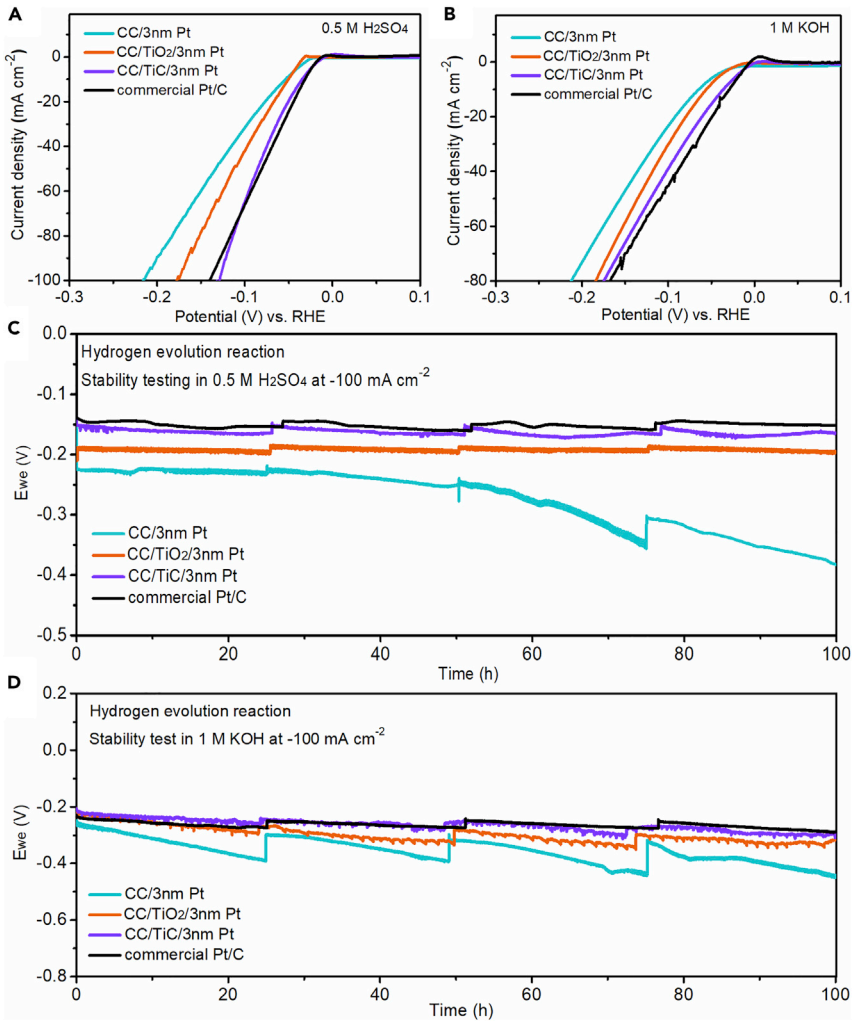

Figure 2. Electrocatalytic Hydrogen Evolution Performance

Linear sweep voltammograms (scanned from negative to positive) at a rate of 1 mV s^{-1} for the CC/Pt, CC/TiO_2/ Pt, CC/TiC/Pt, and commercial Pt/C in (A) 0.5 M H_2SO_4 and (B) 1 M KOH, respectively; chronopotentiograms of CC/Pt, CC/TiO_2/ Pt, CC/TiC/Pt, and commercial Pt/C at a constant current density of −100 mA cm^{-2} in (C) 0.5 M H_2SO_4 and (D) 1 M KOH for 100 h.

little improvement in the catalytic performance on CC/TiO_2 (Figure S4; Table S3), whereas 8 nm Pt on CC/TiC shows slightly better activity than 3 nm Pt on CC/TiC, but it will improve the cost. Thus, 3 nm Pt deposited samples are selected in this work for the further investigation of catalyst stability and solar-driven water splitting.

Our CC/TiC/Pt showed a comparable performance to a commercial Pt/C (10 wt % Pt on carbon black) catalyst loaded on carbon cloth substrate (1 mg cm^{-2} mass loading of Pt) (Figures 2A and 2B). In acidic and basic electrolytes, the commercial Pt/C required overpotentials of 32 and 30 mV respectively to achieve a current density of −10 mA cm^{-2}. The performance of the substrates was also tested for comparison (Figure S5). CC, CC/TiO_2, and CC/TiC exhibited poor activities with respective overpotential >400 mV in KOH and ~200 mV in H_2SO_4 to deliver a current density of −10 mA cm^{-2} (Table S4), confirming that the high electrocatalytic activity of our catalysts arises from anchored Pt nanoclusters.

We further compared the performance of the as-prepared catalysts by evaluating their mass (Pt) normalized activity in 0.5 M H_2SO_4 (Figure S6; Table S5). At an overpotential of 100 mV, we obtained mass-normalized current densities of 237 and 328 mA mg^{-1} Pt for the CC/TiO_2/Pt and CC/TiC/Pt, respectively, which are ~4–5 times higher than that of the commercial Pt/C (67 mA mg^{-1}). This demonstrates the superior activity of Pt nanoclusters supported on TiO_2 and TiC compared to commercial Pt/C catalyst.

We tested the durability of the catalysts by passing a constant cathodic current density of −100 mA cm^{-2} to produce hydrogen for 100 h (Figures 2C, 2D, S7, and S8). The chronopotentiogram for CC/TiC/Pt showed a small increase in the overvoltage from 146 to 154 mV during the electrolysis in an acidic electrolyte, which is comparable to that of the commercial Pt/C (from 138 to 146 mV). In contrast, all the Pt-based catalysts suffered from slight degradation in 1 M KOH. The degradation could be attributed to the poisoning effect of the re-deposited Ni, which originates from the dissolution of Ni foam counter electrode during long-term electrolysis at high current density. Our hypothesis is strongly supported by the appearance of metallic Ni peaks at 44.6° and 51.9° in X-ray diffractograms of Pt-based catalysts after stability test in 1 M KOH (Figure S9). Among these catalysts, commercial Pt/C showed the best resistance toward Ni poisoning, probably due to its largest surface area (Figures S10–S12; Table S6). The SEM images of the catalysts after 100 h stability showed some aggregation in all samples, as seen in Figures S13 and S14. This could be due to the high surface free energy of nanoclusters, which induced the aggregation to form larger clusters or nanoparticles, especially under long-time reaction condition.[32,33]

Here, we attribute the outstanding activity and stability of the Pt-nanocluster-based catalysts to the strong metal-support interaction (SMSI) between Pt atoms and the substrates, which has been demonstrated to occur preferentially in the case of highly dispersed noble metal with small particle size.[34–37] In our TiO_2- and TiC NW-supported catalysts, the existence of the SMSI effect was elucidated by the observed binding energy shift of Pt $4f_{7/2}$ in XPS spectra (Figure S15). The binding energies of all the peaks are determined by referencing them to the C 1s value of 284.8 eV. In both cases, the downshift of Pt 4f core-level, ~0.7 eV on TiO_2 and ~1.0 eV on TiC NWs, indicates an increased electron density, which is attributed to the electron transfer from surface Ti to Pt atoms. Reason for this electron transfer has been ruled out to be the substitution by the Pt atoms of a vacant oxygen or carbon sites during the atomic layer deposition of Pt at high temperature.[36]

We also attribute the good performance of CC/TiO_2/Pt and CC/TiC/Pt partially to the high electrochemical surface area (ECSA) of the titanium-based substrates (Figures S10–S12; Table S6). It is noted our CC/TiC/Pt showed a comparable performance even though its surface area is lower than the commercial Pt/C catalyst. This further suggests that the SMSI effect between our TiC and Pt nanoclusters positively affects the catalytic performance.

Water Electrolysis Driven by Monolithic Perovskite/Silicon Tandem Solar Cell

NiFe LDH delivers an efficient and stable performance toward OER in 1 M KOH, as demonstrated by LSV and chronopotentiometry measurement in Figure S16. Herein, an overall water-splitting electrolyzer was engineered using Pt-based catalysts as the cathode and NiFe LDH as the anode.[15] The distance between the two electrodes was kept at 1 cm to minimize *i*R drop, and 1 M KOH was used as the electrolyte. The electrolyzer based on CC/TiO_2/Pt delivered a current density of 10 mA cm^{-2}

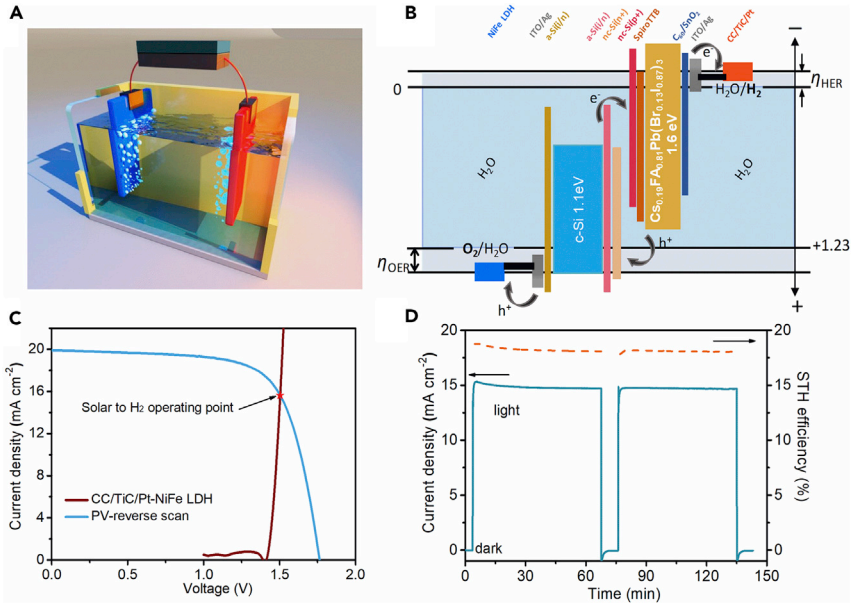

Figure 3. Solar-Driven Water Splitting

(A) Schematic diagram of the solar-driven water-splitting system.

(B) Simplified schematic energy diagram of the perovskite/Si tandem solar cell integrated water splitting.

(C) *J-V* curve of the perovskite/Si tandem solar cell from reverse scan under simulated AM 1.5 G 100 mW cm^{-2} illumination and LSV curve of CC/TiC/Pt and NiFe LDH electrodes based two-electrode configuration. The illuminated surface area of the tandem cell and the electrode was 1.42 cm^2.

(D) Current density-time curve of the solar-driven water splitting device without external bias under chopped simulated AM 1.5 G 100 mW cm^{-2} illumination and the calculated STH conversion efficiency of the integrated device.

at a cell voltage of only 1.51 V (Figure S17A), which was further reduced to 1.48 V using CC/TiC/Pt cathode. Furthermore, the stability of overall water splitting was measured under a constant current density of 100 mA cm^{-2} for 100 h. As shown in Figure S17B, CC/TiC/Pt and commercial Pt/C showed more stable performance than that on CC/TiO_2/Pt as well.

Based on the above highly efficient water-splitting catalysts, here we employed for the first time a perovskite/Si tandem solar cell to drive the water photolysis (Figure 3A).[17] A detailed schematic diagram of the perovskite/Si tandem cell is provided in Figure S18A, of which sub-cell using a $Cs_{0.19}FA_{0.81}Pb(Br_{0.13}I_{0.87})_3$ perovskite solar cell delivered a matched current density of 20.11 mA cm^{-2} with that of Si heterojunction bottom cell (20.55 mA cm^{-2}, Figure S18B). The schematic energy diagram of the integrated overall configuration is shown in Figure 3B. From the *J-V* curve in Figure 3C, the tandem cell used in the integrated device exhibited a J_{sc} of 19.90 mA cm^{-2}, a V_{oc} of 1.76 V and a fill factor of 71.7%, corresponding to a solar to electric power conversion efficiency (PCE) of 25.1% from the reverse curve in standard AM 1.5 G sunlight. Furthermore, the stability of a co-processed perovskite/Si tandem cell was measured at maximum power point (MPP) for 10 h in an ambient air without any encapsulation and the power conversion efficiency (PCE) remained more than 95% after the test (Figure S18C). The intersection of the *J-V* curves of the tandem solar cell with that of the electrolyzer yields a predicted operating current density for the photo-electrolysis system of 15.59 mA cm^{-2} at a voltage of 1.50 V (Figure 3C). We further characterized the

performance of the combined system under AM 1.5 G chopped light illumination without applying any external bias for more than 2 h. (Figure 3D). The system delivered a peak solar-to-hydrogen (STH) conversion efficiency of ~18.7%, which was calculated from the steady-state output of water splitting current density of ~15.20 mA cm^{-2} in the first 5 min, assuming 100% faradic efficiency for hydrogen evolution (see detailed calculation in Experimental Procedures). This performance ranks our system the most efficient PV-driven water splitting employing earth-abundant light-harvesting materials. Furthermore, the perovskite/Si tandem device showed insignificant PCE loss after the water splitting measurement for >2 h (Figure S18D) and an overaged STH conversion efficiency of 18.02% was obtained for the overall system.

DISCUSSION

Downsizing the Pt particles to nanocluster, even single-atom scale, is highly desirable for cost-efficient catalytic reactions. Here, we show that the atomic layer deposition technique enables to uniformly disperse small Pt nanoclusters on CC/TiO_2 and CC/TiC substrates. The use of Ti-based substrates with a high surface area offers a strong metal-support interaction, which plays a critical role in enhancing the activity and stability of our Pt nanocluster catalysts. Wiring a perovskite/Si tandem solar cell directly to an electrolyzer provides a sufficient and quasi-ideal photovoltage for efficient overall water splitting without using any voltage converter, enabling an STH conversion efficiency of 18.7% for the overall system under standard AM 1.5 G illumination.

Future development of photoabsorber and electrolyzer is necessary for scaling up this solar water-splitting technology. Besides the efficiency of photovoltaics that is limited largely by the fill factor and current density, the main challenge is to stabilize the perovskite photoabsorber, which can be achieved by interface passivation, composition engineering, surface protection, and cell encapsulation. For the electrolyzer, novel substrates that enhance the binding of catalysts should be investigated to improve the stability in both acidic and basic electrolytes. Nevertheless, our work demonstrates an efficient solar water splitting system with earth-abundant light-harvesting material and efficient electrocatalysts.

EXPERIMENTAL PROCEDURES

General

All solutions used in this work were prepared with 18.2 MΩ·cm deionized water from a Millipore system (Purelab Ultra, ELGA). All the chemicals were used without purification unless otherwise stated.

ALD Synthesis of TiO_2

TiO_2 was deposited on carbon cloth (0.33 mm, CeTech Co., Ltd) by atomic layer deposition (ALD, Savannah 11, Cambridge Nanotech), using tetrakis-dimethylamino titanium (TDMAT) and deionized water as the Ti and O precursor, respectively. The carbon cloth was placed inside the chamber of ALD after being cleaned with ozone-UV for 15 min. The deposition temperature was 150°C, while the container for the TiO_2 precursor was kept at 75°C. The thickness of TiO_2 substrate was controlled by adjusting the number of ALD cycles. Typically, 510 cycles deposition yielded 30-nm-thick TiO_2 film. Then the TiO_2-coated carbon cloth was moved into a tube furnace (Thermo Scientific) and heated to 900°C at a heating rate of 10°C·min^{-1} with continuous flow of argon (99.9999%, Carbagas). After 3 h calcination, the furnace was allowed to cool naturally to room temperature.

Preparation of TiC NWs

TiC NWs were prepared by a templating method adapted from a previous work.[38] Briefly, 160 mg of TiO_2 powder (anatase, <25 nm, 99.7%, Aldrich), 58 mg of NaCl and 30 mg of $Ni(NO_3)_2 \cdot 6H_2O$ were dissolved in 10 mL of ethanol to form a Ni–Ti–Cl emulsion under ultrasonication. Then, 300 mg carbon cloth (pre-cut into several 13 × 100 mm rectangles) was dipped in the Ni–Ti–Cl emulsion. After magnetic stirring overnight, the carbon cloth was dried at 60°C for 2 h in a pre-heated oven to remove ethanol. The nickel-, chlorine-, and Ti-loaded carbon cloth was placed between two slices of titanium foam and placed inside a graphite crucible, which was covered with a graphite lid. Then the samples were heated to 1,250°C in a tube furnace at a heating rate of $5°C \cdot min^{-1}$ under a continuous 100 sccm flow of pure Ar gas. After 3 h calcination, the furnace was turned off and allowed to cool naturally to room temperature. To purify the synthesized TiC NWs surface and reduce the possible intermediate TiO_x phase, the samples were placed in a new graphite crucible, without titanium foam and graphite lid, and calcined for 3 h at 1,250°C (at a heating rate of $5°C \cdot min^{-1}$) under a continuous flow of 5% H_2/95% Ar gas mixture. After 3 h calcination, the furnace was allowed to cool naturally to room temperature.

Preparation of Pt Catalysts

The Pt nanoclusters were deposited onto the surface of substrates by atomic layer deposition (ALD, Beneq TFS200, Finland). $MeCpPtMe_3$ (98%, Aldrich) and ozone (99.99%, Carbagas) were used as precursors of Pt and O, and nitrogen (99.9999%, Carbagas) was used as the purge gas. The deposition temperature was 280°C, and the container for $MeCpPtMe_3$ was kept at 75°C, providing a steady flux of $MeCpPtMe_3$ vapor. In each cycle, 0.5 s of $MeCpPtMe_3$ pulse and 0.5 s of O_3 pulse were separated by 2 s of N_2 purge. The Pt loading on different substrates was accurately controlled by the number of ALD cycles. ALD of Pt follows a similar pathway as CVD of Pt during the oxidative decomposition of $MeCpPtMe_3$,[39] but separating into two half-reaction:

1st half-reaction:

$$Pt\text{-}O^* + (MeCp)Pt(CH_3)_3 \rightarrow (CH_3)_2Pt(MeCp)^* + CO_2 + H_2O + \text{fragments}.$$

2nd half-reaction:

$$(CH_3)_2Pt(MeCp)^* + O_2 \rightarrow Pt\text{-}O^* + CO_2 + H_2O + \text{fragments}.$$

Here, * represents an active surface species, and Pt-O* represents oxygen molecules that are adsorbed on the Pt surface.

NiFe-Layered Double Hydroxide Catalyst Fabrication

The NiFe-layered double hydroxide (LDH) was fabricated by hydrothermal growth according to previous reports but with a modified recipe.[15] Briefly, 0.3 g $Ni(NO_3)_2$ (≥99%, Fluka), 0.6 g $Fe(NO_3)_2$ (>99.99%, Sigma-Aldrich) and 0.3 g urea ($CO(NH_2)_2$, 99.8%, Sigma-Aldrich) were mixed in 80 mL of deionized water to prepare a homogenous solution. Then the solution was poured into a 100 mL autoclave with a piece of Ni foam (>99.5%, 1.5 mm, Taiyuan Yingze Lizhiyuan Battery) leaned against the wall. The growth was carried out at 120°C in an electric oven for 6 h. After allowing the autoclave to cool naturally to room temperature, the samples were removed, washed with deionized water, and then dried under a stream of compressed air.

Physical Characterization

The morphologies and microstructures of the as-prepared catalysts were examined by a scanning electron microscope (SEM, ZEISS Merlin) and transmission electron microscope (TEM, FEI Osiris). X-ray diffraction (XRD) was performed via Bragg-Brentano Geometry with a Lynexeye detector and a monochromated Cu Kα radiation source. X-ray photoelectron spectroscopy was carried out using a PHI VersaProbe II XPS microprobe. The spectra are calibrated using C 1s peak at 284.8 eV and fitted using mixed Gaussian-Lorentzian function with XPSPEAK software.

Electrochemical Measurements

The electrochemical properties of the catalysts were tested using a computer-controlled SP-200 (BioLogic Science Instruments) with a three-electrode system that consists of a Ni foam counter electrode (in alkaline condition) or carbon cloth counter electrode (in acid condition) and Ag/AgCl (saturated with KCl, Pine) reference electrode. The electrolyte was 1 M KOH or 0.5 M H_2SO_4. The activity toward hydrogen evolution reaction (HER) was characterized by linear sweep voltammetry (LSV) at a scan rate of 1 mV s^{-1}, and the scan direction was from negative to positive potential. Similarly, the performance toward oxygen evolution reaction (OER) of NiFe LDH was measured by LSV at a scan rate of 1 mV s^{-1} in 1 M KOH. The stability of the Pt-based catalysts and NiFe LDH toward HER and OER was characterized by applying −100 and 100 mA cm^{-2} constant current density for 100 h, respectively. For the two-electrode water splitting measurement, the overall reaction was characterized by LSV at a scan rate of 1 mV s^{-1} from 2 to 0 V. The stability of overall water splitting was characterized by chronoamperometry applying 100 mA external bias for 100 h.

Photovoltaic-Driven Water Splitting Characterization

The monolithic perovskite/silicon heterojunction (perovskite/Si) tandem solar cell was prepared as described in a previous work.[17] Here, a two-lamp solar simulator (Xenon and Halogen, class AAA, Wacom) was used to accurately measure perovskite and silicon solar cells (including UV and IR components). Three independently certified silicon heterojunction cells (by F-ISE) were used to calibrate our solar simulator, among which two cells with blue and red filter integrated respectively to the encapsulation frame and the other without light filter. Using the filter integrated cells, the light contribution in the red and blue area can be finely tuned, and the current thus was measured separately. The third certified cell (without filter) is used to calibrate the total intensity to standard solar irradiation (100 mW cm^{-2}). The temperature of the perovskite/Si tandem cell was kept at 25°C during the overall measurement using a temperature-controlled stage. A shadow mask was used to define the illuminated area (1.42 cm^2). The J-V curves were measured at a scan rate of 100 mV s^{-1} (using an integration time of 0.1 s and a delay of 0.1 s for each data point, the voltage step was 0.02 V). The performance of the solar-driven water splitting was recorded by chronoamperometry without applying an external bias under chopped AM 1.5G illumination. The active area of the water splitting catalytic electrodes was 1.42 cm^2 as well.

ECSA Calculation

The ECSA of the catalysts was determined from the double-layer capacitance through cyclic voltammetry at different scan rates in 0.5 M H_2SO_4. The potential range where no apparent faradic processes occur was selected.[40] The double-layer charging current i_c, for the CC/TiC/3 nm Pt and CC/TiO_2/3 nm Pt catalysts, was measured from CVs at multiple scan rates. The charging current is equal to the product of the scan rate, v, and the electrochemical double-layer capacitance, C_{dl}:[41]

$$i_c = vC_{dl}.$$

Thus, a plot of i_c as function of v yields a straight line with a slope equal to C_{dl}:[40]

$$\mathrm{ECSA} = \frac{C_{dl}}{C_s},$$

where C_s is the specific capacitance of the sample or the capacitance of an atomically smooth planar surface of the materials per unit area under identical electrolyte conditions. For our estimates of roughness factor, we use general specific capacitances of C_s = 30 μF cm^{-2} in 0.5 M H_2SO_4 for Pt.

Calculation for the Pt Loading Amount

In terms of the loading amount of Pt nanoclusters on three substrates, we hypothesis that Pt form a uniform film on the whole surface of three substrates. The volume (v) of the deposited Pt nanoclusters is:

$$v = h \times S_{sub} \times R_F,$$

where h is the deposited thickness of Pt nanoclusters, and S_{sub} and R_F are the geometric surface area and roughness factor of the substrate. R_F of three substrates was calculated by measuring the double-layer capacitance. The loading amount can be calculated using the following equation:

$$\text{Pt loading} = \frac{\rho \times v}{S_{sub}} = \frac{\rho \times h \times S_{sub} \times R_F}{S_{sub}} = \rho \times h \times R_F,$$

where ρ is the density of the Pt. Here, we take CC/3 nm Pt catalyst as an example:

$$\text{Pt loading} = \rho \times h \times R_F = 21.45\ \mathrm{g\ cm^{-3}} \times 3 \times 10^{-7}\mathrm{cm} \times 31 = 0.199\ \mathrm{mg\ cm^{-2}}.$$

STH Conversion Efficiency Calculation

For the overall water splitting system that produces hydrogen and oxygen molecules using only solar power as the input, the solar-to-hydrogen conversion efficiency (STH) is defined as:

$$\mathrm{STH} = \frac{\text{Chemical energy output}}{\text{Solar energy input}} = \frac{j_{op} \times A \times E_f \times FE_{H_2}}{P_s \times A}$$

Here, j_{op} represents the operating current density of the combined system, A is the effective illuminated area, E_f is the standard thermodynamic potential difference between hydrogen evolution and oxygen evolution half-reactions (1.23 V) that is corresponded to the change of Gibbs free energy of overall water splitting, FE_{H_2} is the faradic efficiency for hydrogen evolution that is assumed to be 100% and P_s is the power of solar illumination.

SUPPLEMENTAL INFORMATION

Supplemental Information can be found online at https://doi.org/10.1016/j.joule.2019.10.002.

ACKNOWLEDGMENTS

This work was supported by the National Key Research and Development Program of China (no. 2018YFB1502003), the Strategic Japanese–Swiss Science and Technology Programme from the Swiss National Science Foundation (no. 514259), the PECHouse3 project from the Swiss Federal Office of Energy (no. SI/500090-03), the Sino-Swiss Science and Technology Cooperation (SSSTC) 2016 project from the Swiss National Science Foundation (project no. IZLCZ2–170294), the Chinese Thousand Talents Program for Young Professionals (J.L.), the Overseas

Expertise Introduction Project for Discipline Innovation of Higher Education of China (111 Project, grant no. B16027), and the China Scholarship Council (CSC) (file no. 201706370233, J.G.). M.G and S.M.Z thank the King Abdulaziz City for Science and Technology (KACST) for financial support. F.S. and C.B. acknowledge the financial support of the Swiss National Science Foundation via NRP70 Energy Turnaround PV2050 and Swiss National Science Foundation Bridge (176552) projects.

AUTHOR CONTRIBUTIONS

J.L. and M.G. designed and supervised the project. J.G. prepared the Pt nanocluster catalysts and performed the electrochemical and solar-driven water-splitting test. F.S., J.W., Q.J., and C.B. provided the monolithic perovskite/silicon tandem solar cell. C.L. synthesized the TiC nanowire array samples on carbon cloth. J.L. conducted the electron microscopy measurements. S.M.Z. helped with the coordination of the work. J.G., J.L., and D.R. wrote the first draft, and M.G. and J.L. finalized the manuscript. All authors discussed the results and contributed to the manuscript.

DECLARATION OF INTERESTS

The authors declare no competing interests.

Received: July 23, 2019
Revised: September 8, 2019
Accepted: October 1, 2019
Published: October 25, 2019

REFERENCES

1. Jamesh, M.I. (2016). Recent progress on earth-abundant hydrogen evolution reaction and oxygen evolution reaction bifunctional electrocatalyst for overall water splitting in alkaline media. J. Power Sources *333*, 213–236.

2. Chu, S., and Majumdar, A. (2012). Opportunities and challenges for a sustainable energy future. Nature *488*, 294–303.

3. Cook, T.R., Dogutan, D.K., Reece, S.Y., Surendranath, Y., Teets, T.S., and Nocera, D.G. (2010). Solar energy supply and storage for the legacy and nonlegacy worlds. Chem. Rev. *110*, 6474–6502.

4. Wang, H., and Dai, H. (2013). Strongly coupled inorganic–nano-carbon hybrid materials for energy storage. Chem. Soc. Rev. *42*, 3088–3113.

5. Walter, M.G., Warren, E.L., McKone, J.R., Boettcher, S.W., Mi, Q., Santori, E.A., and Lewis, N.S. (2010). Solar water splitting cells. Chem. Rev. *110*, 6446–6473.

6. Turner, J.A. (2004). Sustainable hydrogen production. Science *305*, 972–974.

7. Zeng, K., and Zhang, D. (2010). Recent progress in alkaline water electrolysis for hydrogen production and applications. Prog. Energy Combust. Sci. *36*, 307–326.

8. Holladay, J.D., Hu, J., King, D.L., and Wang, Y. (2009). An overview of hydrogen production technologies. Catal. Today *139*, 244–260.

9. Kim, J.H., Hansora, D., Sharma, P., Jang, J.W., and Lee, J.S. (2019). Toward practical solar hydrogen production–an artificial photosynthetic leaf-to-farm challenge. Chem. Soc. Rev. *48*, 1908–1971.

10. Jia, J., Seitz, L.C., Benck, J.D., Huo, Y., Chen, Y., Ng, J.W.D., Bilir, T., Harris, J.S., and Jaramillo, T.F. (2016). Solar water splitting by photovoltaic-electrolysis with a solar-to-hydrogen efficiency over 30%. Nat. Commun. *7*, 13237.

11. Nakamura, A., Ota, Y., Koike, K., Hidaka, Y., Nishioka, K., Sugiyama, M., and Fujii, K. (2015). A 24.4% solar to hydrogen energy conversion efficiency by combining concentrator photovoltaic modules and electrochemical cells. Appl. Phys. Express *8*, 107101.

12. Bonke, S.A., Wiechen, M., MacFarlane, D.R., and Spiccia, L. (2015). Renewable fuels from concentrated solar power: toward practical artificial photosynthesis. Energy Environ. Sci. *8*, 2791–2796.

13. Cheng, W.-H., Richter, M.H., May, M.M., Ohlmann, J., Lackner, D., Dimroth, F., Hannappel, T., Atwater, H.A., and Lewerenz, H.-J. (2018). Monolithic photoelectrochemical device for direct water splitting with 19% efficiency. ACS Energy Lett. *3*, 1795–1800.

14. NREL (2019). Best research-cell efficiency chart. https://www.nrel.gov/pv/cell-efficiency.html.

15. Luo, J., Im, J.H., Mayer, M.T., Schreier, M., Nazeeruddin, M.K., Park, N.G., Tilley, S.D., Fan, H.J., and Grätzel, M. (2014). Water photolysis at 12.3% efficiency via perovskite photovoltaics and Earth-abundant catalysts. Science *345*, 1593–1596.

16. Schüttauf, J.-W., Modestino, M.A., Chinello, E., Lambelet, D., Delfino, A., Dominé, D., Faes, A., Despeisse, M., Bailat, J., Psaltis, D., et al. (2016). Solar-to-hydrogen production at 14.2% efficiency with silicon photovoltaics and earth-abundant electrocatalysts. J. Electrochem. Soc. *163*, F1177–F1181.

17. Sahli, F., Werner, J., Kamino, B.A., Bräuninger, M., Monnard, R., Paviet-Salomon, B., Barraud, L., Ding, L., Diaz Leon, J.J.D., Sacchetto, D., et al. (2018). Fully textured monolithic perovskite/silicon tandem solar cells with 25.2% power conversion efficiency. Nat. Mater. *17*, 820–826.

18. Lu, Z., Zhu, W., Yu, X., Zhang, H., Li, Y., Sun, X., Wang, X., Wang, H., Wang, J., Luo, J., et al. (2014). Ultrahigh hydrogen evolution performance of under-water "superaerophobic" MoS_2 nanostructured electrodes. Adv. Mater. Weinheim *26*, 2683–2687, 2615.

19. Liao, L., Wang, S., Xiao, J., Bian, X., Zhang, Y., Scanlon, M.D., Hu, X., Tang, Y., Liu, B., and Girault, H.H. (2014). A nanoporous molybdenum carbide nanowire as an electrocatalyst for hydrogen evolution reaction. Energy Environ. Sci. *7*, 387–392.

20. Popczun, E.J., McKone, J.R., Read, C.G., Biacchi, A.J., Wiltrout, A.M., Lewis, N.S., and Schaak, R.E. (2013). Nanostructured nickel phosphide as an electrocatalyst for the hydrogen evolution reaction. J. Am. Chem. Soc. *135*, 9267–9270.

21. Kuang, Y., Feng, G., Li, P., Bi, Y., Li, Y., and Sun, X. (2016). Single-crystalline ultrathin nickel nanosheets array from in situ topotactic

reduction for active and stable electrocatalysis. Angew. Chem. Int. Ed. Engl. *55*, 693–697.

22. Wang, Y., Zhang, G., Xu, W., Wan, P., Lu, Z., Li, Y., and Sun, X. (2014). A 3D nanoporous Ni–Mo electrocatalyst with negligible overpotential for alkaline hydrogen evolution. ChemElectroChem *1*, 1138–1144.

23. Zhang, H., Li, Y., Zhang, G., Xu, T., Wan, P., and Sun, X. (2015). A metallic CoS_2 nanopyramid array grown on 3D carbon fiber paper as an excellent electrocatalyst for hydrogen evolution. J. Mater. Chem. A *3*, 6306–6310.

24. Seh, Z.W., Kibsgaard, J., Dickens, C.F., Chorkendorff, I., Nørskov, J.K., and Jaramillo, T.F. (2017). Combining theory and experiment in electrocatalysis: insights into materials design. Science *355*, eaad4998.

25. Turner, M., Golovko, V.B., Vaughan, O.P., Abdulkin, P., Berenguer-Murcia, A., Tikhov, M.S., Johnson, B.F., and Lambert, R.M. (2008). Selective oxidation with dioxygen by gold nanoparticle catalysts derived from 55-atom clusters. Nature *454*, 981–983.

26. Herzing, A.A., Kiely, C.J., Carley, A.F., Landon, P., and Hutchings, G.J. (2008). Identification of active gold nanoclusters on iron oxide supports for CO oxidation. Science *321*, 1331–1335.

27. Lei, Y., Mehmood, F., Lee, S., Greeley, J., Lee, B., Seifert, S., Winans, R.E., Elam, J.W., Meyer, R.J., Redfern, P.C., et al. (2010). Increased silver activity for direct propylene epoxidation via subnanometer size effects. Science *328*, 224–228.

28. Vajda, S., Pellin, M.J., Greeley, J.P., Marshall, C.L., Curtiss, L.A., Ballentine, G.A., Elam, J.W., Catillon-Mucherie, S., Redfern, P.C., Mehmood, F., et al. (2009). Subnanometre platinum clusters as highly active and selective catalysts for the oxidative dehydrogenation of propane. Nat. Mater. *8*, 213–216.

29. Qiao, B., Wang, A., Yang, X., Allard, L.F., Jiang, Z., Cui, Y., Liu, J., Li, J., and Zhang, T. (2011). Single-atom catalysis of CO oxidation using Pt1/FeOx. Nat. Chem. *3*, 634–641.

30. Conway, B.E., and Tilak, B.V. (2002). Interfacial processes involving electrocatalytic evolution and oxidation of H_2, and the role of chemisorbed H. Electrochim. Acta *47*, 3571–3594.

31. Pentland, N., Bockris, J.O., and Sheldon, E. (1957). Hydrogen evolution reaction on copper, gold, molybdenum, palladium, rhodium, and iron. J. Electrochem. Soc. *104*, 182–194.

32. Gates, B.C., Flytzani-Stephanopoulos, M., Dixon, D.A., and Katz, A. (2017). Atomically dispersed supported metal catalysts: perspectives and suggestions for future research. Catal. Sci. Technol. *7*, 4259–4275.

33. Corma, A., Concepción, P., Boronat, M., Sabater, M.J., Navas, J., Yacaman, M.J., Larios, E., Posadas, A., López-Quintela, M.A., Buceta, D., et al. (2013). Exceptional oxidation activity with size-controlled supported gold clusters of low atomicity. Nat. Chem. *5*, 775–781.

34. Fung, S.C. (1982). XPS studies of strong metal-support interactions (SMSI)-Pt/TiO/sub 2. J. Catal. *2*, 76.

35. Bahl, M., Tsai, S., and Chung, Y.-W. (1980). Auger and photoemission investigations of the platinum-SrTi O 3(100) interface: Relaxation and chemical-shift effects. Phys. Rev. B *21*, 1344.

36. Horsley, J.A. (1979). A molecular orbital study of strong metal-support interaction between platinum and titanium dioxide. J. Am. Chem. Soc. *101*, 2870–2874.

37. Koudelka, M., Monnier, A., Sanchez, J., and Augustynski, J. (1984). Correlation between the surface composition of Pt/TiO_2 catalysts and their adsorption behaviour in aqueous solutions. J. Mol. Catal. *25*, 295–305.

38. Qiu, Z., Huang, H., Du, J., Tao, X., Xia, Y., Feng, T., Gan, Y., and Zhang, W. (2014). Biotemplated synthesis of bark-structured TiC nanowires as Pt catalyst supports with enhanced electrocatalytic activity and durability for methanol oxidation. J. Mater. Chem. A *2*, 8003–8008.

39. Sun, S., Zhang, G., Gauquelin, N., Chen, N., Zhou, J., Yang, S., Chen, W., Meng, X., Geng, D., Banis, M.N., et al. (2013). Single-atom catalysis using Pt/graphene achieved through atomic layer deposition. Sci. Rep. *3*, 1775.

40. McCrory, C.C., Jung, S., Peters, J.C., and Jaramillo, T.F. (2013). Benchmarking heterogeneous electrocatalysts for the oxygen evolution reaction. J. Am. Chem. Soc. *135*, 16977–16987.

41. Trasatti, S., and Petrii, O.A. (1991). Real surface area measurements in electrochemistry. Pure Appl. Chem. *63*, 711–734.